Key Points:
- The iMARS web-GIS is an open source-based web mapping application that is specialized on surface change analysis on Mars
- It provides dedicated tools for visualization of topography data sets and coregistered multitemporal images as time series
- Case studies show exemplary analyses of equatorial and polar areas with surface change features in their specific context

The Web-Based Interactive Mars Analysis and Research System for HRSC and the iMars Project

S. H. G. Walter[1] , **J.-P. Muller**[2] , **P. Sidiropoulos**[2] , **Y. Tao**[2] , **K. Gwinner**[3], **A. R. D. Putri**[2] ,
J.-R. Kim[4], **R. Steikert**[1], **S. van Gasselt**[1,4,5] , **G. G. Michael**[1] , **G. Watson**[2], and **B. P. Schreiner**[1]

[1] Department of Geosciences, Institute for Geological Sciences, Planetary Sciences and Remote Sensing, Freie Universität Berlin, Berlin, Germany, [2] Department of Space and Climate Physics, Mullard Space Science Laboratory, University College London, Surrey, UK, [3] Institute of Planetary Research, German Aerospace Center (DLR), Berlin, Germany, [4] Department of Geoinformatics, University of Seoul, Seoul, Republic of Korea, [5] Now at National Chengchi University, Taipei, Taiwan

Abstract Web-based planetary image dissemination platforms usually show outline coverage of available data and offer querying for metadata as well as preview and download. While the usual form of presenting multiorbit data sets is to merge the data into a larger mosaic, for change detection purposes it is essential to maintain the individual images as an important snapshot of the planetary surface taken at a specific time. We introduce the web-based interactive Mars Analysis and Research System (iMARS web-GIS), which is specialized on planetary surface change analysis with novel tools for simultaneous visualization of single images as time series in their original sequence. As the data foundation, we use the vast quantity of automatically coregistered orthoimages and digital terrain models (DTM) from three NASA missions' instruments processed and ingested in the context of the EU-funded iMars project. The baseline for the coregistered images are the High-Resolution Stereo Camera (HRSC) multiorbit quadrangle image mosaics, which are based on bundle block-adjusted multiorbit DTM mosaics. Additionally, we make use of the existing along-track bundle-adjusted HRSC single images and DTMs available at the planetary data archives. We provide two science cases for exemplary workflows of the multitemporal single-image analysis, demonstrating the dedicated tools for surface change interpretation—one near Mawrth Vallis and one near the south pole. A web mapping application including the presented functionality has been implemented and is available at http://imars.planet.fu-berlin.de with the iMars project website (http://www.i-mars.eu/web-gis) serving as a mirror.

Plain Language Summary We present a web-based mapping system for Mars with the emphasis on the analysis of change detection features. It contains topographic base maps in an intuitive click, browse, and zoom environment. Single images from the available archive of most past and current space missions can be arranged as stacks and viewed as time series of the recent Martian's surface history. We use the system for two scientific case studies, one from an equatorial region currently under investigation for landing site selections of future rover missions, one from the south pole—known for its continuous annual growth and retreat of polar ice.

1. Introduction and Background

The precise coregistration of the various planetary remote sensing data sets is fundamental for researchers to analyze data combinations with the desired properties, for example, filtered by radiometric, spatial, or spectral resolution, or to examine repeat coverage of a surface feature in different observations. With recent ground resolutions of 0.3 meter per pixel (m/px) and better, coordinate and registration accuracies have become more important than in the past, if pixel-scale coregistration precision is desired. For example, Tao et al. (2016) found misregistrations of 100 to 200 m between High-Resolution Imaging Science Experiment (HiRISE) and High-Resolution Stereo Camera (HRSC) imagery. HRSC provides the unique capability of delivering along-track multistereo digital terrain model (DTM) data of better than 100 m/px with precisely coregistered orthoimages aiming for global coverage. Tied to the global reference system of the Mars Orbiter Laser Altimeter (MOLA) data set, HRSC products play a unique role as an intermediary geometric reference data set linking MOLA to other stereo data sets with higher ground resolution such as the Context Camera (CTX) and HiRISE (Gwinner et al., 2016). iMars is a European Union Research and Innovation project funded

under the 7th Framework Programme focused on developing tools and value-added data sets to massively increase the exploitation of existing image and DTM data sets of Mars (Muller et al., 2016). Within the project, efforts for the creation of precisely coregistered planetary data products of available past and present Mars missions have led to a new archive of DTMs (Tao et al., 2018) and time series of images covering the same areas multiple times (Sidiropoulos et al., 2018). For the exploitation of the newly available data, automatic data mining of change detection features have been performed (Sidiropoulos & Muller, 2017, results currently in preparation) and validated using crowd-sourcing techniques (Sprinks et al., 2016a, 2016b). Besides these background tasks, the iMars project provides a window to the public — with new concepts for the analysis of the rich data sets with their special spatiotemporal aspects in a dedicated web-based Geographic Information System (web-GIS).

Current browser-based platforms for planetary image dissemination and analysis usually show outline coverage of various data sets and offer querying for metadata as well as preview and download, for example, the *Mars Orbital Data Explorer* (ODE; Wang et al., 2009), the *Planetary Image Locator Tool* (PILOT; Bailen et al., 2013), and the *HRSC MapServer* (Walter & van Gasselt, 2014). *Mars Trek* (Law & Day, 2017) has recently been expanded beyond its original design as a public outreach tool and offers a great variety of data layers and analysis functions. Besides some of them allowing regular filtering for start/stop time attributes, these tools do not provide dedicated functionality for temporal image analysis. The web-based multitemporal database *MUTED* (Heyer et al., 2018) is designed to support the identification of surface changes and shows outlines of overlapping images from two different selectable instruments. It has the capability to determine repeat images from a user-defined time span to query possible coverage of surface changes caused by very short-term and temporally variable processes like dust devils. The system links to the preview images of the data in separate windows, but the images themselves are not displayed in the map or shown aligned to each other — making it hard to compare the same feature on two different images in the browser. That means there is still an essential amount of manual work necessary to download, process, and coregister the image data before the user is then able to analyze the respective surface areas for possible temporal changes. The stand-alone JAVA application *JMars* (Christensen et al., 2009) allows rendering of single images in the map view, but only one at a time, which makes it impractical for surface change visualization. *PlanetServer* (Marco Figuera et al., 2018), a set of tools for hyperspectral data visualization and analysis has sophisticated functionality for rendering the images in the map, but has no options for temporal analysis. As none of the systems use coregistered imagery but nominal spacecraft pointing data, one would also expect wrong results of overlapping images due to the already mentioned misregistrations. With regard to Earth-based systems, *GloVis Next* (https://glovis.usgs.gov) recently introduced the concept of full-resolution preview images rendered into the map view, with basic time filtering possibilities. Designed as a preview site for selection and download of images only, built-in tools for image sort ordering and dynamic time series visualization of the images are not included. Landsat-based data with the recurrent Path/Row-based WRS2 system would be predestined for time series visualization. The *MEA/EarthServer* service (https://eodataservice.org) provides temporal analysis with dedicated tools for data cubes and a timeline where available single images can be selected. But in the planetary domain, images are rarely available as data cubes due to their heterogenous acquisition geometries.

To achieve change detection visualization functionality for planetary application, we want to be able to display all images available from a certain spot on the surface in their full spatial resolution — and to show them together animated as a time series. In-depth analysis of the data requires functionality such as switching quickly between layers, known as flickering (in the case of two layers of images) or cycling (more than two layers). In this paper we describe these new concepts and the development of the web-based interactive Mars Analysis and Research System (iMARS web-GIS) for scientists and the public with special functions dedicated to the spatiotemporal visualization of the newly available DTMs and image products. It is available online at http://imars.planet.fu-berlin.de and (as a mirror) under the official iMars project website at http://www.i-mars.eu/web-gis.

2. Materials and Methods

The iMARS web-GIS comprises a browser-server infrastructure, which loads dynamic code from a website and connects to web services of a server-based backend. The web services stream preprocessed data from connected databases and storage subsystems according to the standards of the OGC (Open Geospatial Consortium, 2002, 2006, 2010), adapted for planetary reference systems (Hare et al., 2018).
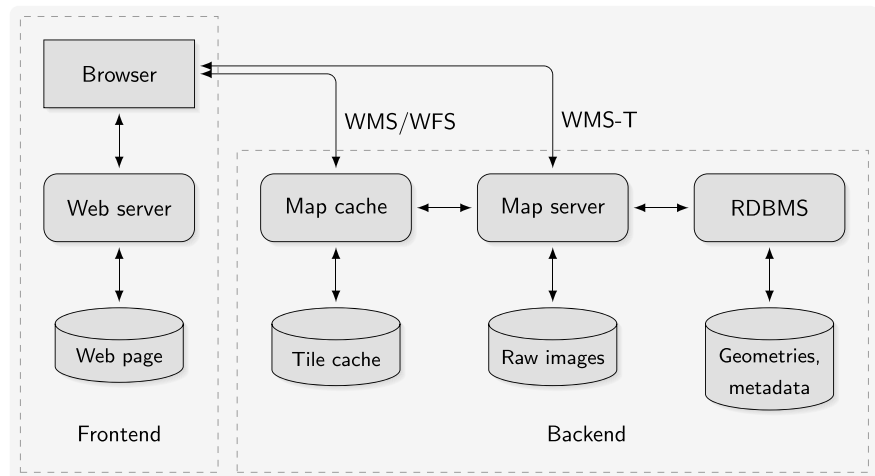
Figure 1. System design of the iMARS web-GIS outlining frontend (client) and backend (server) components.

2.1. General System Design

We use a client-server infrastructure as the general system design with the web browser representing the client. The iMARS web content (HTML, CSS) including dynamic code (JavaScript) is retrieved from a web server, gets executed in the browser, and dynamically streams the topography, image, and vector data from the server backends. Therefore, we differentiate between the frontend and the backend of the system, with the stored web page on the server logically still belonging to the frontend side of the system, as it is interpreted on-the-fly and launched on the client (Figure 1). The client code consists of the map canvas with user interface components, including attribute filter masks and data layer selection components. The selected data layers are requested directly from the map cache instance via concurrent OGC-based Web Map Service (WMS) and Web Feature Service (WFS) calls.

The backend parts consist of a map cache, a map server, a relational database management system (RDBMS), and local storage systems. For requests without time filtering, the client communicates mainly with the map cache—if data are missing in the cache, the request is forwarded to the map server. Only in the special case of time-filtered WMS requests (WMS-T), the browser gets the tiles directly from the map server as configuring the cache with time as a dimensional parameter is currently not supported. The details and linked web addresses of the existing software packages used are listed in a dedicated table in the supporting information to this article. We use *MapServer* for its performance-oriented design using C code as its basis. It is connected to the *Apache* web server via the Common Gateway Interface (CGI) using *fastCGI* for performance-efficient connections. For the map cache, we use the *MapCache* software configured as an Apache module. *PostgreSQL* with the *PostGIS* extension is used as the spatial database backend. In our case the software components of the whole infrastructure reside on the same physical machine but the design allows to spread the services on separate machines for achieving performance gains from the balanced loads. The system has been built by using solely open source software, and the additional developments are published together with this article.

2.2. Spatiotemporal Queries

As a tool dedicated to change detection, the iMARS web-GIS is focused on the acquisition time of the images—therefore, all backends are time aware and images are attached with time stamps in the databases. The methods for using client-server-based streaming protocols for the transfer of imaging and geometry data filtered by time are well established by the service standards definitions of the OGC. For performance considerations, wherever possible, the time constraints are included in the request to the server. When the requests are processed on the server and only the requested parts of data are streamed to the client, we minimize the amount of data which has to be transferred to and filtered on the client. For the display and selection of geometric outlines of the available data, we use either WMS for streaming the data as bitmaps or WFS for streaming the data as vector data including attributes. As WFS responses are not cached by the map cache, the requests are handed over to the map server instance (cf. Figure 1). Although slower due to the lack of tile caching and the requirement of being processed in the client, WFS requests are needed for advanced filtering of special attributes such as the solar longitude. As the regular WMS spatial reference systems (SRS)

still rest upon the Earth-based definitions from the European Petroleum Survey Group (EPSG), which are not valid for planetary SRSs, we define pseudo codes of the EPSG name space combined with the NAIF codes similar to the ones used by Hare et al. (2018), with the difference that we do not use the IAU2000 Areoid, but the MOLA sphere (radius 3,396.0 km) instead. In the cases where we provide WMS/WFS interfaces to external clients directly, MapCache offers the possibility to define aliases to any other possible existing SRS namespace.

2.3. Dynamic WMS Layers

Due to the vast number of single images we needed a way to set up the layers in a dynamic way since the map server does not know the images to be served beforehand. This requires an additional parameter associated with the Planetary Data System (PDS) product ID (a unique identifier available for all NASA and ESA mission data products). In the OGC definition, such nonstandard parameters providing enhanced capabilities can be realized as vendor-specific parameters (VSPs; Open Geospatial Consortium, 2002). To provide dynamic layers, we introduce the `PRODUCTID` parameter in the WMS request to the map server. To ensure compatibility with regular WMS, the service will produce a valid result using a predefined default if the `PRODUCTID` parameter is omitted or malformed.

The dynamic service is implemented as a *MapScript* instance of MapServer. MapScript connects the Apache web server to the MapServer application programming interface using CGI and provides an interface for the Python language, among others. When used in the context of OGC services, it is capable of intercepting the request and using the request parameters for further processing. We use internal map template configurations with incomplete file paths for each available dynamic layer representing a camera instrument. With the product ID provided as an additional parameter, the internal path to the requested image on disk is constructed and the map is then finally configured. In this way, the individual layers are created on-the-fly, each representing only one single image. On the frontend side, the VSP request parameter (`PRODUCTID`) has to be appended to the regular set of WMS parameters. The pool of available product IDs is constructed from the requested attributes of the footprint coverage query on the frontend. Therefore, a coverage query always has to precede the single-image query and visualization.

It has to be considered that each dynamic single-image request is handled as a separate processing thread on the server; therefore, large numbers of requested images will result in a large server load. To minimize the waiting time and improve the user experience, the dynamic single-image mechanism can also be covered by the map cache. MapCache offers the configuration of additional dimensions for the tileset, enabling the possibility of having multiple dimensions inside one layer. When configured as such, the value of the `PRODUCTID` parameter gets appended to the cache path on the disk, so that each image has its separate cache target space. The cache will then be seeded during runtime on its first call or alternatively using a separate preseeding call for every image. The complete data flow of the described WMS request and its response is shown in Figure 2.

The WMS request is received by the Apache web server at an address configured for the MapCache module. In case the requested tile is available in the tile cache, it is retrieved from the cache and immediately committed to the client. If it is not available, the tile request is forwarded back to Apache to the WMS source address configured with the MapScript CGI script. The Python script intercepts the WMS request and extracts the product ID from the parameter chain. It loads the layer object from the map file and appends the file name and path of the required image. After some possible further image processing inside the script (e.g., stretching or color matching), the request is submitted to the MapServer backend which in turn delivers the response back to the MapCache instance. An additional advantage of this workflow in terms of system security is that the WMS source address is never visible to the outside, only via the MapCache instance.

For external data queries and access, we have successfully extended the dynamic WMS services and implemented the Europlanet Data Model Table Access Protocol (EPN-TAP; Erard et al., 2014) to provide Virtual Observatory (VO) access to the single HRSC *granules* via WMS (cf. Minin et al., 2016). As a first step, the single HRSC Level-3 images are available in Equidistant Cylindrical projection and can be queried by attribute keywords or geometry. Therefore, the Python scripts have been extended to produce dynamic `GetCapabilities` output with available images as individual layers. Several utilities for data mining and analysis can connect now to these data sources via well-defined standard interfaces for VOs. Entry points are http://vespa.obspm.fr for web-based query forms or http://dachs.planet.fu-berlin.de for the Astronomical Data Query Language (ADQL) used by the VO infrastructure (Quinn et al., 2004).
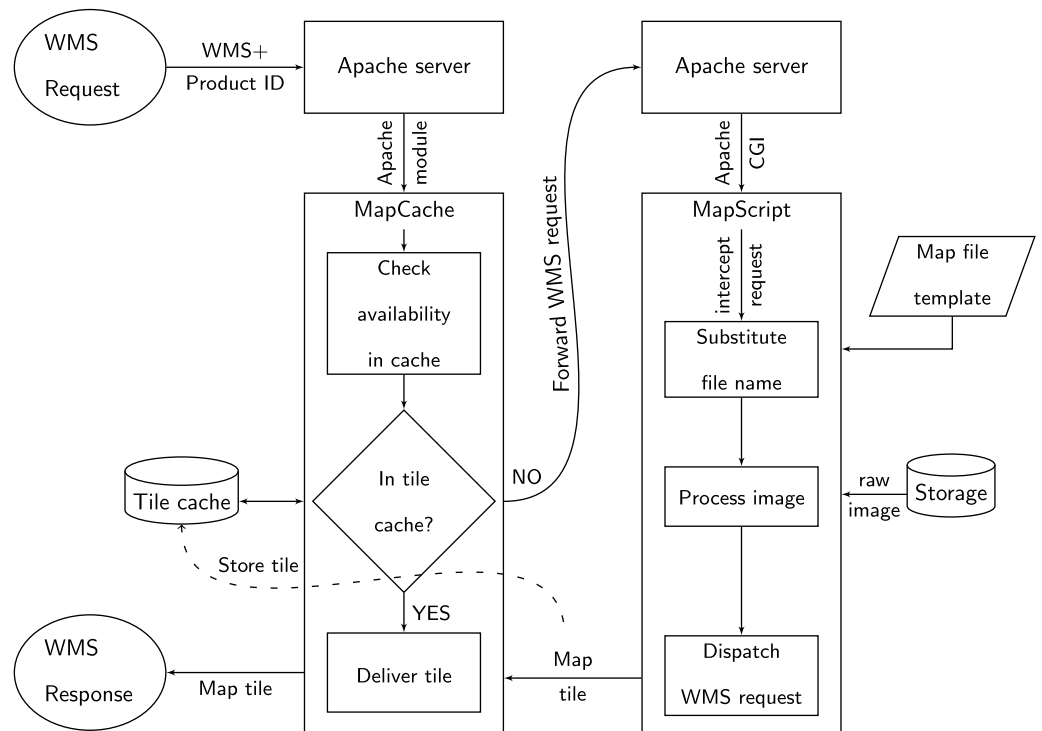
Figure 2. Data flow of the described WMS request of a single image together with its PDS product ID keyword and the resulting response.

2.4. Data Structures and Preprocessing

A summary of all the available topographic and imagery data sets available in the iMARS web-GIS is given in Table 1.

Besides the indirect usage of the MOLA data in data processing pipelines of other data sets, we use the Mission Experiment Gridded Data Record (MEGDR) as a background layer, PDS data set ID `MGS-M-MOLA-5-MEGDR-L3-V1.0` (Smith et al., 2003). For the equatorial view of the web-GIS (in Equidistant Cylindrical projection) the highest-resolved MOLA topography data has 128 pixels per degree (ppd) with an equivalent

Table 1
Topographic and Imagery Layers in the Web-Mapping System, Sorted by Grid Size in Descending Order

Instrument	Description	Extent	Coverage	Grid size [m/px]
Topography data (DTMs)				
MOLA	MOLA mission experiment gridded data record (MEGDR)-equatorial	−88° to 88° lat	99.9%	463
MOLA	MOLA mission experiment gridded data record (MEGDR)-south polar	−73.2° lat	2.1%	115
HRSC	Single strips, bundle adjusted (ba), coregistered to MOLA	global	53.1%	50−200
HRSC	Multiorbit mosaic, bundle block adjusted (bba), coregistered to MOLA	MC-11	3.1%	50
CTX	Single strips, coregistered to HRSC	global	0.6%	~18
HiRISE	Single strips, coregistered to HRSC	global	≪0.1%	0.75−1.0
Image data (HRSC baseline and ACROs)				
HRSC	Single strips, orthorectified on ba DTMs	global	53.1%	12.5−100
HRSC	Multiorbit mosaic, orthorectified on bba HRSC DTM (panchromatic/color)	MC-11	3.1%	12.5/50
THEMIS	Single strips, orthorectified on MOLA and coregistered to HRSC	MC-11	2.2%	17.5−70
CTX	Single strips, orthorectified on MOLA and coregistered to HRSC	MC-11	2.5%	5−6
MOC-NA	Single strips, orthorectified on MOLA and coregistered to HRSC	MC-11	0.1%	1−12

Note. The single-strip image data are available as dynamic layers of time series.
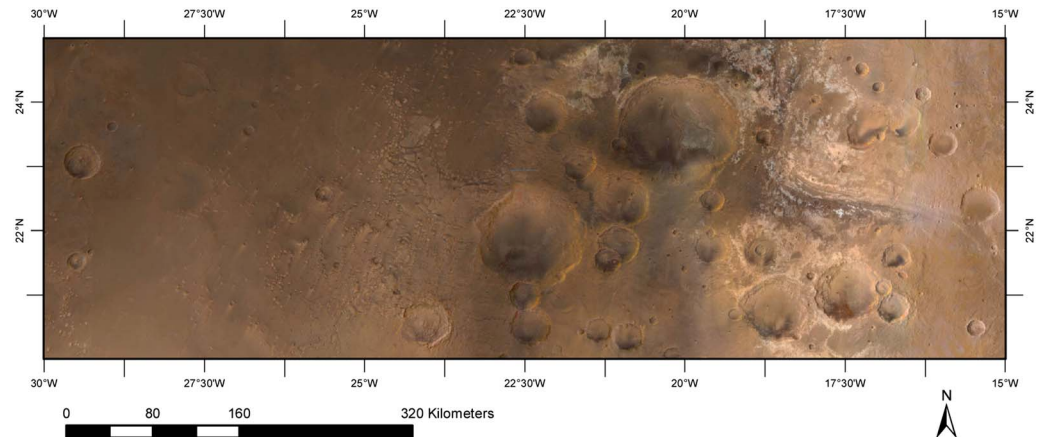
Figure 3. Detailed view of a subset of the MC11 quadrangle image mosaic in the transition area between MC11-E and MC11-W (the half-quadrangle border is in the center of the image at 22°30″W).

of 463.08 m/px at the equator. For the polar data, we use the available higher-resolved data set with 512 ppd , respectively 115.09 m/px in the center of the projection. The data labels have been corrected for slight inconsistencies in the projection offsets—the label entries LINE_PROJECTION_OFFSET and SAMPLE_PROJECTION_OFFSET are in error by 1 px in several label files throughout the whole data set (as documented, e.g., in the ISIS3 source code). The MOLA spheroid with the height reference value of 3,396.0 km is derived from the IAU1991 coordinate system (Smith et al., 2001). To conform with HRSC, for the poles, we converted the reference values from 3,372 to 3,396.0 km.

The different kinds of HRSC image and DTM data products serve as the reference data sets to which all other iMars data sets are coregistered. HRSC Level-4 data include DTMs derived from stereo photogrammetry and bundle adjustment (ba, along-track between the five different panchromatic channels) as well as orthorectified images to these DTMs (Gwinner et al., 2010). Up to level 4, all data are published as single-sequence (*single-strip*) data products related to their initial orbit configuration during image acquisition. In contrast, the soon to be published HRSC level 5 products are sets of multiorbit data products derived from several adjacent and overlapping single-strip data products. The level 5 products consist of the multiorbit DTM mosaic with a cell size of 50 m/px, created using additional cross-track bundle block adjustment techniques and tied to MOLA (Gwinner et al., 2016). Along with the DTM, multiorbit image mosaics are produced with resolutions of 12.5 m/px (panchromatic) and 50 m/px (color, Figure 3), respectively. Before mosaicking, the single images are photometrically corrected (Lambertian assumption) to remove brightness variations due to varying illumination during acquisition (Walter et al., 2015) and radiometrically tied to the Thermal Emission Spectrometer bolometric albedo map (Christensen et al., 2001) as a global brightness standard. Before feathering into a homogeneous mosaic, manual sorting and contrast enhancement are applied (Michael et al., 2016).

In the web-GIS, the HRSC image and topography data are available as grouped layers of static base layers. Users have the choice between separate layers for the panchromatic and the color mosaic product, respectively. The level 5 mosaics are currently not available elsewhere, but it is intended by the HRSC team to publish them in ESA's Planetary Science Archive (PSA) and NASA's PDS archives (Gwinner et al., 2016). The panchromatic mosaic is stored in its original form as a 16-bit file—the stretching to 8 bit is performed on-the-fly by the MapServer application. The stretch is done globally on a static per data set basis (same values applied over the whole extent). Despite its large file sizes (about 80 GB for the panchromatic, 12 GB for the color image mosaic of the whole quadrangle), the display in the client is very fluent due to the efficient map tile cache instance in between the map server and the client browser.

Multiresolution coregistered DTMs are essential to improve our understanding of the Martian surface formation processes. Although the University of Arizona (UoA) has produced 726 HiRISE DTMs to date (Kirk et al., 2008), the UoA DTMs only cover a tiny percentage of the Martian surface (≪1%) and most of them do not contain repeat observations. We investigated several planetary DTM pipelines, none of them meeting the quality and speed requirement for batch processing of large amount of CTX and HiRISE stereo images. Subsequently within the iMars project, we developed the automated multiresolution coregistered DTM processing
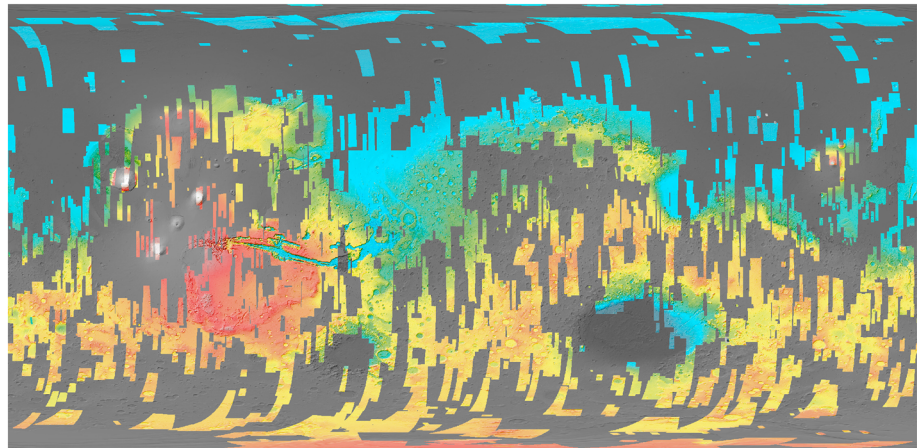
Figure 4. The topographic background layer groups combine coregistered terrain data from four different instruments (cf. Table 1) with cell grid sizes ranging from 463 m/px (MOLA) to 50 m/px (HRSC) to 18 m/px (CTX) and down to less than 1 m/px (HiRISE). MOLA = Mars Orbiter Laser Altimeter; HRSC = High-Resolution Stereo Camera; CTX = Context Camera; HiRISE = High-Resolution Imaging Science Experiment.

chain for CTX and HiRISE stereo pairs, called the Coregistration Ames Stereo Pipeline Gotcha Optimised (CASP-GO). CASP-GO is built on the open source NASA Ames Stereo Pipeline (Broxton & Edwards, 2008; Moratto et al., 2010), tie point-based multiresolution image coregistration (Tao et al., 2016), and the Gotcha subpixel refinement method (Tao & Muller, 2016). The implemented system (Tao et al., 2018) guarantees global georeferencing compliance with respect to HRSC, and hence to MOLA, providing refined stereo matching completeness and accuracy. The developed CASP-GO system has then been used to produce ∼5,000 CTX stereo images to date and around 30 HiRISE DTMs for areas with five or more repeat views using Microsoft® Azure® cloud computing resources, which are currently being evaluated (Tao et al., 2018). Around 350 of the processed CASP-GO CTX DTMs have been ingested into the web-GIS. The CTX and HiRISE DTMs will be continuously updated on the website as soon as new DTMs become available from the cloud computing resources. We plan to link against the actual data product downloads once the DTMs are available in the PDS archive. A by-product in the DTM generation process are Ortho-Rectified Images (ORI) registered to the CASP-GO DTMs. These are arranged as a dedicated group under the static base image layers in the web-GIS. Global sets of CTX and HiRISE ortho images are available as single layers. As we found no outliers in the data, the images are stretched to 8 bit (from float, originally) using a simple min/max stretch.

The multiorbit HRSC mosaic, using sophisticated techniques as described earlier, is currently only available for the MC-11 quadrangle. As a global topography data set we have merged all released single-strip HRSC level 4 DTMs into a large file with a grid size of 50 m/px. In the web-GIS it is available together with the other HRSC DTMs as separate layers in a dedicated group. The HiRISE and CTX DTMs have also been merged to be shown as separate layers in a particular group. The individual iMars product-related DTM layers are shown as color-hillshades with a uniform color ramp over the whole height range. The MOLA DTM base layer is shown as a grayscale hillshade with all the other data sets on top—in the order of the resolution of the data sets, best resolution on top. With all data sets coded with the same color scheme and the better resolved data set always overlaying the lower-resolution one, we can achieve a uniform browsing experience being able to zoom in from the global view down to less than 1 m/px within the same data set. As appearing in the frontend (Figure 4), these layers are composed dynamically on the map server. We have prerendered the hillshade files, the color ramps are overlaid on-the-fly (allowing modification of the color scheme).

NASA images have been processed using the Automatic Coregistration and Orthorectification (ACRO) pipeline, which was developed within the iMars project (Sidiropoulos & Muller, 2018) and employs novel image matching strategies for working with large volumes of multiinstrument planetary image data sets, and geometric modeling to process NASA images from Viking Orbiter to CTX. ACRO can be applied using as a baseline either single-strip HRSC level 4 DTMs and orthoimages, or HRSC mosaics (Sidiropoulos et al., 2018), or a hybrid combination of CTX ORIs and HRSC DTMs. In order to discard images in which the ACRO pipeline failed to process without producing severe artifacts, their visual quality is automatically assessed and low-quality products are flagged. Nearly 6,800 NASA images from MOC-NA, THEMIS and CTX, coregistered to the HRSC

image mosaic of the MC-11 quadrangle, have been provided for use in the web-GIS. During ingestion, all the single images were preprocessed with regard to transparency (null) values, bit depth conversion, and pyramid creation. As artifact outliers are often present in the regular processing pipeline for the THEMIS-VIS and MOC-NA data, we use a 4 sigma stretch instead of a regular min/max stretch when converting from 16 bit to 8 bit. The preprocessed images are located in structured subfolders and are streamed into the client interface by the methods described in section 2.3.

For the query functionality based on attributes, we collect metadata early in the processing pipeline using the Integrated Software for Imagers and Spectrometers, version 3 (ISIS3) of the U.S. Geological Survey's Astrogeology Science Center (Keszthelyi et al., 2013). We use text files with parameter value line syntax and Python to dynamically create necessary tables in PostgreSQL database and seed the tables with the metadata entries. Due to the different metadata, for example, MOC and CTX we maintain individual tables for each instrument type available as ACRO images. For the footprints of the HRSC images, we use our already existing database containing extended attribute information, which is systematically updated on the arrival of new images (Walter et al., 2006). As PostGIS, a geospatial extension by PostgreSQL, by default, only supports the common EPSG set of Coordinate Reference Systems, we register the three used projections (Equidistant Cylindrical and North/South Polar Stereographic) in the internal `spatial_ref_sys` table. Although the used Coordinate Reference Systems do not follow the IAU2000 convention, we still use the NAIF-based coding scheme for the Spatial Reference Identifier as proposed by Hare et al. (2006), where Mars is defined as "499" and two additional digits determine the projection. Following this proposal, we use the Spatial Reference Identifiers 49900 for the spheroid definition, 49910 for the Equidistant Cylindrical projection, 49918 for the North Polar, and 49920 for the South Polar Stereographic projection, respectively.

2.5. Frontend

The frontend is based on the *OpenLayers* (OL) JavaScript library in version 3 updated to the latest available minor version (the recent major version increase to OpenLayers 4 made parts of our code incompatible, but we plan to correct this). OpenLayers provides a web map canvas with additional basic user interface elements for map interaction, such as panning, zooming, and full-screen controls. Since its transition from version 2 to version 3, the OpenLayers maintainers have abandoned providing high-level functionality such as the *layer switcher* element. Instead, they recommend third party developers to maintain their own add-on libraries. For the layer management user interface we used the *ol-LayerSwitcher* by Matt Walker and adapted it for additional functionality such as group folding/unfolding, transparency sliders and automatic/manual layer sorting and removal. Attribute query results are shown as pop-up windows on the map with the use of the unmodified *ol-Popup* module from the same author. For the graphical icons of the adapted LayerSwitcher module we have made use of the *Font Awesome* font repository. The *Bootstrap* JavaScript library has been used for modal windows of the info button functionality. For the switching between the global Equidistant Cylindrical projection and the Polar Stereographic projections we have made use of the *ol3-projection-switcher* module from University of Colorado's National Snow and Ice Data Center.

Besides enhancing preexisting OL modules, we have created additional interface elements from scratch based on the pure OL framework, such as the *Time panel* for temporal filtering and the ortho-image *Workflow toolbar* for visualizing single images. An additional user interface element allows direct coordinate entry from the keyboard resulting in movement of the map center to the entered point ("*Goto lat, lon*"). For computations converting Earth dates to Martian years and back again, we use the JavaScript code from the web site of *Laboratoire de Météorologie Dynamique* (http://www-mars.lmd.jussieu.fr). The numbering scheme of the Martian years is based on the calendar proposed by Clancy et al. (2000) where Mars year 1 (MY 1) begins on 11 April 1955, at a time such that solar longitude $Ls = 0$. A Martian year has 668.6 Martian solar days (Sol), begins with Sol 1 and ends with the rounded Sol 669.

With the methods presented above we have implemented a fully functional web-GIS infrastructure consisting of server backends (web server, cache server, map server, database server) and a client frontend (running JavaScript code in the browser). All available data produced from within the iMars project have been included together with other available data sets useful for providing additional context. Navigation is provided by an interactive pan-, zoom-, and click environment common to all user interface elements placed on the actual

Figure 5. Browser view of the iMARS web-GIS with the user interface controls shown (numbered in red): 1 = Zoom controls; 2 = Fullscreen control; 3 = Goto lat,lon; 4 = Time panel; 5 = Projection switcher; 6 = Layer switcher; 7 = Workflow toolbar. The current extent's ACRO and HRSC baseline images available for time series visualization are shown as black outlines. iMARS web-GIS = interactive Mars Analysis and Research System; ACRO = Automatic Co-registration and Orthorectification; HRSC = High-Resolution Stereo Camera.

map canvas (see Figure 5). It is beyond the scope of this publication to describe the system and its components in every detail. Instead, we want to describe the necessary user interactions for an exemplary work flow for the visualization of time series of single images. For this example, we use an image extent over an unnamed crater (diameter ~23 km) north of Aram Dorsum at 11.4°W 9.1°N but of course, any other area with available ACRO/HRSC multiple coverage will work as well.

As a first step, footprints of at least one instrument have to be activated inside the "Orthoimage footprint" group of the Layer switcher (top-most group of user interface element no. 6 in Figure 5). Generally, the Workflow toolbar is operated by clicking the buttons from left to right. For a detailed view showing all buttons of the Workflow toolbar available in the public version of the web-GIS, see Figure 6. By clicking the *info* button of the toolbar (button no. 1 in Figure 6), the attribute query mode is started—clicking on a footprint outline queries the backend for available attributes at that specific point, and a popup window containing the queried information from the available metadata catalog is shown. Button no. 2 enables the *single select* function. If this button is enabled, choosing geometries of active layers of the "Orthoimage footprint" group selects the footprints and shows the selected outlines in different colors. The next two active buttons allow the automatic zoom to the extent of the selected images (button no. 3 in Figure 6) and the disabling of the colorized selection outlines (button no. 4). Button no. 5 removes the selection and resets the state of the toolbar to the default. To load the images from a nonempty selection, press button no. 6 (labeled *create layers*). The dynamic "Orthorectified images" group is then added on top of the list of layers and filled with layers representing the selected images. By *hovering* over an image ID (keeping the mouse over the name without clicking), attributes of the image (Earth date, resolution, and Ls) are displayed in a popup frame. It is possible to change the layer sorting inside the group from time-based to name- or resolution-based sorting with the respective buttons. Usually, the next step is to go through the images and inspect them one by one on image quality, brightness and resolution. If one image for any reason does not fulfill the needs, it can be removed with the *ban* button next to the respective image ID. With the video playback tools (Figure 6, nos. 7 and 8) it is possible to show each single image after the other in a loop cycle. This way, existing changes become immediately visible. The playback can be paused at any image or stopped with the respective buttons (the pause button appears only while playing). A typical view of an active work session for dynamic single-image layer visualization is shown in Figure 7.
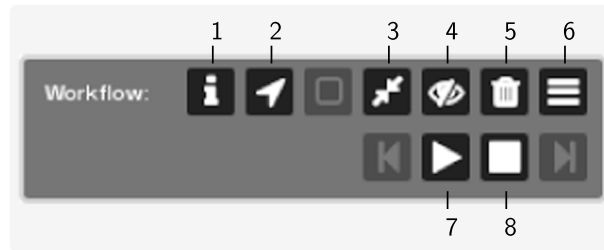
Figure 6. The graphical user interface element "Workflow toolbar" allows navigating through the available tools for dynamic single-image visualizations — all functional buttons are shown. Buttons are numerated and their respective functionality is explained in the text. The functionality of the grayed-out buttons is not available in the public version of the web-GIS.

3. Science Cases and Results

To allow a better understanding of the value of the iMARS web-GIS to the scientific community, in the following, we provide two case studies of real-world analysis examples.

3.1. Aeolian Deposits Near Mawrth Vallis

The quadrangle MC-11 "Oxia Palus" currently hosts the majority of coregistered image and DTM data provided within the iMars project. It is located to the west of the Martian prime meridian and covers 45° in the east-west and 30° in the north-south direction. The quadrangle contains the Mawrth Vallis region known for some of the largest outcrops of phyllosilicate-rich rocks on Mars (Poulet et al., 2005). In the west the quadrangle contains the Arabia Terra region, characterized by dark material deposits on bright floors of craters (Figure 8). Surface changes of the accompanied dark streaks have already been observed between Mariner 6 (1969), Mariner 9 (1972), and Viking 2 (1976–1980) (Thomas & Veverka, 1979). We were able to locate and visualize recent changes within an intracrater dark unit south of Mawrth Vallis (red square in Figure 8). The crater floor of an unnamed crater with 11 km diameter shows a low albedo unit in its center.

In total, at the location there are 12 separate images available from different instruments at different acquisition times (see Table 2). Using the video playback functionality of the iMARS web-GIS toolbar, it becomes apparent that the areas of low albedo significantly change in size and distribution over the years of recorded
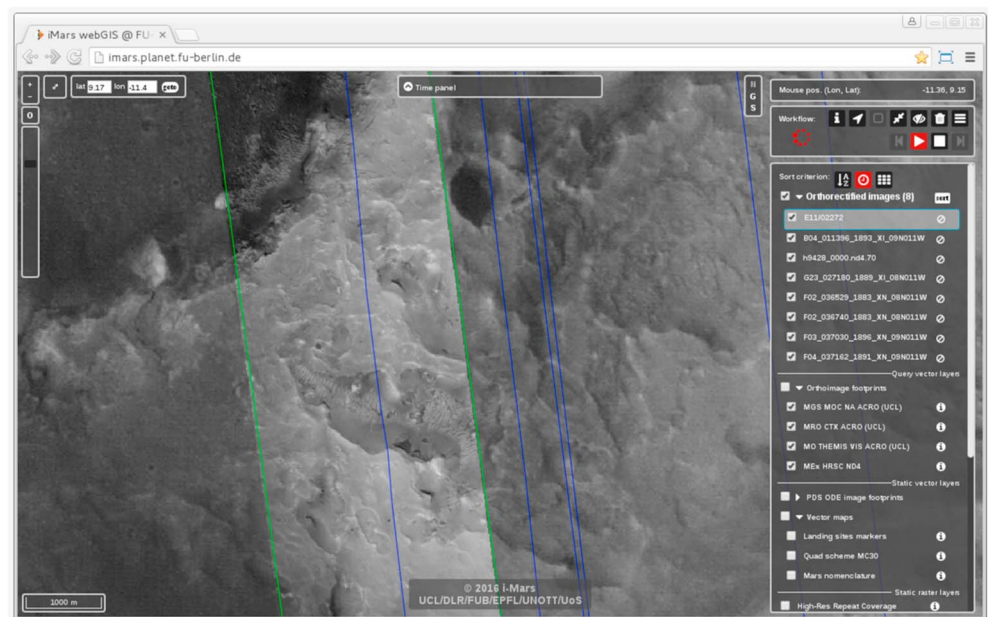

Figure 7. Snapshot of selected single images from HRSC and coregistered images from MOC and CTX. The available single-image coverage is shown in the Layer switcher (right side of the figure) and the respective images are cycled by the activated video player function (top right). HRSC = High-Resolution Stereo Camera.
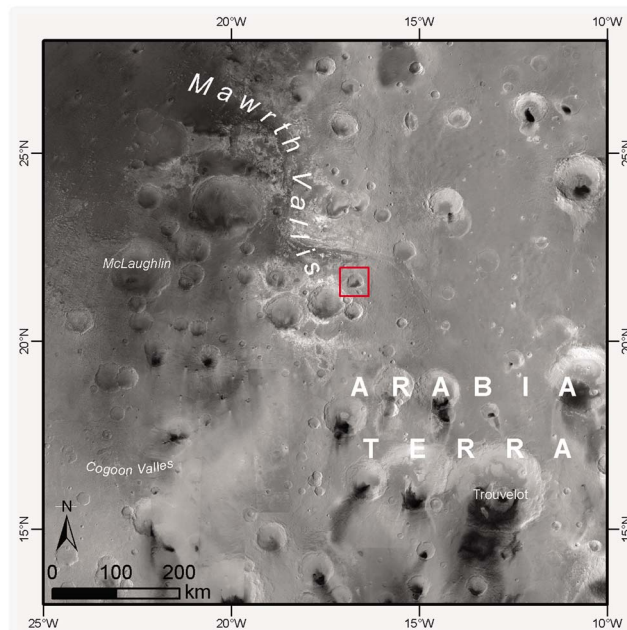
Figure 8. Context of the area of investigation (red square) for surface change visualization and analysis. Background: HRSC image mosaic from MC11. HRSC = High-Resolution Stereo Camera.

imagery. The available images cover a time range of 10 Earth years and more than five Martian years. As listed in the table, some of the images were acquired very closely after each other.

We could observe two major changes of the distribution of the dark area between MY 27/Sol 566 and MY 29/Sol 29 and between MY 29/Sol 301 and MY 31/Sol 153, as well as a minor change between MY 32/Sol 69 and MY 32/Sol 224. During the first change the dark area expands to the southwest, during the second it further spreads to the northwest, and the third change shows again a decimation of dark material (Figure 9). The third change is not completely unambiguous as Figure 9c appears overall darker than Figure 9d and in general the images are not corrected for photometric and atmospheric effects, as they have been acquired under different illumination (and atmospheric) conditions. Present activity is proven in the form of a dust devil

Table 2

Available Images at the Investigation Site at 21.6° N, 16.6° W Are Listed in Chronological Order Together With the (Earth) Date of Acquisition and Their Corresponding Martian Year and Solar Day

| Product ID	Instrument	Earth date	MY	Sol
V11921009LOC	THEMIS-VIS	2004/8/21	27	164
H2196_0001.ND4	HRSC	2005/9/29	27	557
H2229_0001.ND4	HRSC	2005/10/8	27	566
H5163_0009.ND4	HRSC	2008/1/8	29	29
H5181_0000.ND4	HRSC	2008/1/14	29	35
P16_007111_1997_XN	CTX	2008/2/1	29	52
B02_010394_2026_XI	CTX	2008/10/14	29	301
HA359_0000.ND4	HRSC	2012/2/17	31	153
HC423_0000.ND4	HRSC	2013/10/10	32	69
D22_035817_1999_XI	CTX	2014/3/18	32	224
F01_036094_1999_XI	CTX	2014/4/8	32	244
ESP_037017_2015	HiRISE	2014/6/19	32	307

Note. Dates are formatted as year/month/day.
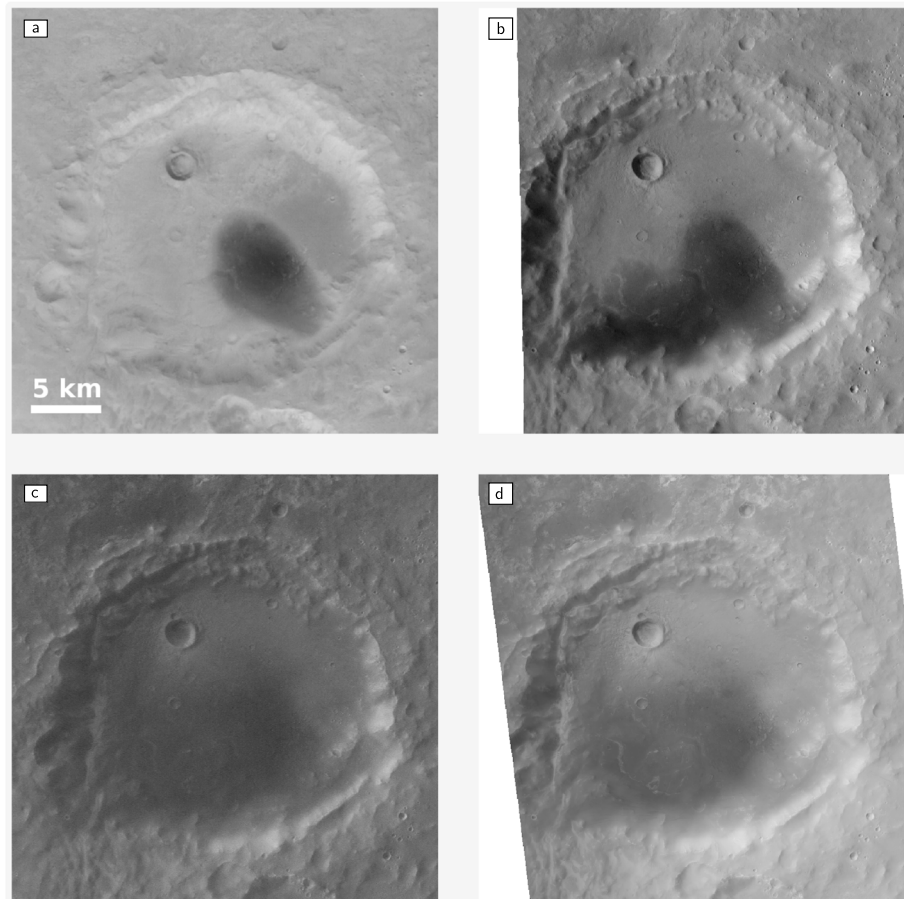
Figure 9. Low albedo unit in a crater South of Mawrth Vallis, located at 21.6°N, 16.7°W. Series of four identical subsets of images from different acquisition times in chronological order. (a) HRSC sequence H2229_0001 acquired on 8 October 2005. (b) HRSC sequence H5163_0009 acquired on 8 January 2008. (c) HRSC sequence HC423_0000 from 10 October 2013. (d) CTX image F01_036094_1999_XI_19N016W from 8 April 2014. Differing illumination directions for all images.

in the northwest of Figure 9b. For an animation of all available images from within the iMARS web-GIS as seen by the user after activating the video playback functionality, refer to the supporting information of this paper.

At first sight, it appears that the dark material consists of low-albedo sand transported by eolian processes into the crater. This scenario is often found in the surrounding craters of the Arabia Terra region (e.g., Edgett & Malin, 2000). Being able to zoom in and out on the stack of various images enables a wider view of the scene. A more detailed look at the dark area on the crater floor from the CTX imagery with nearly 5 m/px resolution clearly shows its ancient origin as being heavily cratered (see Figure 10a). One candidate in the stratigraphy could be the dark, unaltered capping unit uniformly draped over the Noachian plateaus regardless of topography described by Loizeau et al. (2012). A distinct relatively younger crater on the brighter part of the surface in Figure 10a (white arrow) shows dark ejecta rays around it, which indicate that it is the brighter material being deposited above the dark unit. The available HiRISE image exhibits bright dust filling inside dark craters with bright dust-composed transversal dunes (Figure 10b). This clearly indicates that the changes visible during the observed recent time scales are related to the transport of bright dust deposited on top of the dark cratered unit, instead of dark sand being transported on top of a bright unit.

This example demonstrates that for the detailed analysis of such morphologic features it is necessary to interactively work with the available images simultaneously in their different levels of resolution and detail. That is, a context image is necessary for the general shape and distribution of the albedo variations. Detailed views are essential for the analysis of small-scale features like craters and eolian deposits. The preprocessed and coregistered images within the iMARS web-GIS enable immediate analysis of the data without any further manual processing required by the users.
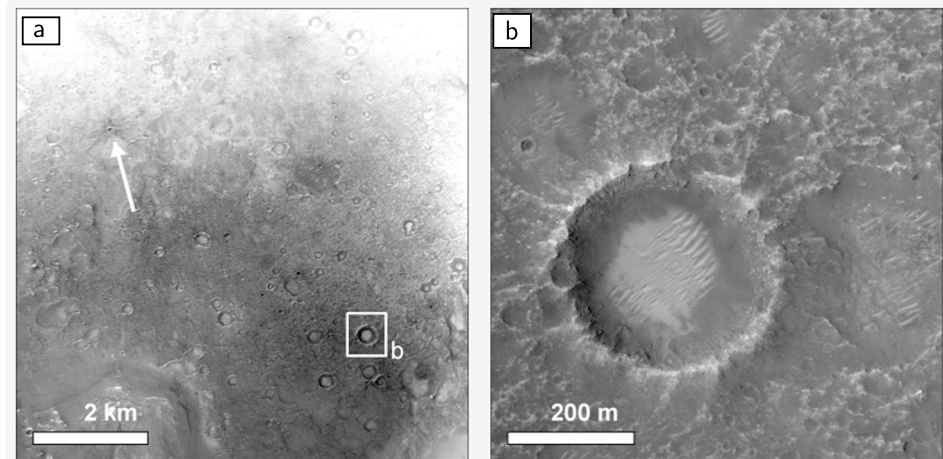
Figure 10. Details of the low-albedo crater floor of Figure 9. (a) CTX image F01_036094_1999_XI showing a fresh impact with dark ejecta rays (white arrow) and outline of Figure 10b. (b) HiRISE image ESP_037017_2015 showing bright sandy dunes inside the darker crater. CTX = Context Camera; HiRISE = High-Resolution Imaging Science Experiment.

3.2. Seasonal Changes at the South Polar Cap

The polar caps of Mars are among the most dynamic areas on the planet and therefore most promising for the detection of short-term surface change features. The main driver for the changes is the annual growth (by condensation) and retreat (by sublimation) of the seasonal ice caps, a thin layer of CO_2 ice overlaying the polar layered deposits, which themselves are proposed to be composed of airborne dust, possibly sand, and water ice precipitated from the atmosphere (Piqueux et al., 2003). At the south pole, several features indicating surface changes have been observed in the past. These are periodically appearing features on the seasonal cap and perennial features visible after the seasonal cap has completely disappeared. Among the seasonal features are polygonal patterns, dark spots and fans as well as generally low-albedo areas termed the *cryptic* region, most of which are attributed to gas venting mechanisms where CO_2 gas and dust is involved (Kieffer, 2007; Kieffer et al., 2006; Piqueux & Christensen, 2008). Perennial circular depressions known as *Swiss cheese terrain* are found on the south polar residual cap and are monitored continuously by the MOC and HiRISE instruments (James et al., 2007). In the locations where the seasonal features formed during the phase of sublimation of the CO_2 ice, spider-like features and polygonal troughs can be observed, once the seasonal cap has entirely disappeared (Piqueux & Christensen, 2008). The extent and variability of the caps themselves have been recently described for eight Martian years (MY 24 to 31) by Piqueux et al. (2015) using the MGS Thermal Emission Spectrometer and MRO Mars Climate Sounder (MCS) thermal infrared data. At the south pole, Calvin et al. (2017) reported about the extent of the seasonal polar cap and specifically the cryptic region over a period of four Martian years (MY 28 to 31) using the MRO Mars Color Imager data.

The creation of HRSC level 4 DTMs of the Martian south pole (Putri et al., 2016a) will be the base for future coregistered image products from CTX and HiRISE (Putri et al., 2016b). In the meantime, we have processed all available HRSC images covering the south pole and orthorectified the data using the 512 ppd MOLA DTM. The (currently) 356 images in South Polar Stereographic projection together with the equatorial HRSC level 3 image data from the PSA/PDS archives in Equidistant Cylindrical projection are available in an updated version of the HRSC Mapserver (Walter & van Gasselt, 2014) at http://maps.planet.fu-berlin.de., based on the software presented here. Due to the large variety of the HRSC data and because of the orbital configuration of the spacecraft and the periodically changing ice coverage, we have integrated filter sliders for the solar longitude Ls and the spatial resolution of the HRSC images. This allows studies of interannual variations by comparison of images from the same Ls but from different Martian years as well as studies of seasonal variability by comparing images from within the same Martian year but different Ls. The iMARS web-GIS has particular tools for displaying both kind of observations and building time series as animations, which allows excellent comparison of the data within a couple of clicks. In the following, we will give two examples for HRSC observations of both seasonal and interannual variations.

Between December 2014 and May 2015 an HRSC *broom calibration* campaign was performed, a maneuver where all sensors are slewed over the surface and therefore recording it at the same observation angle. The
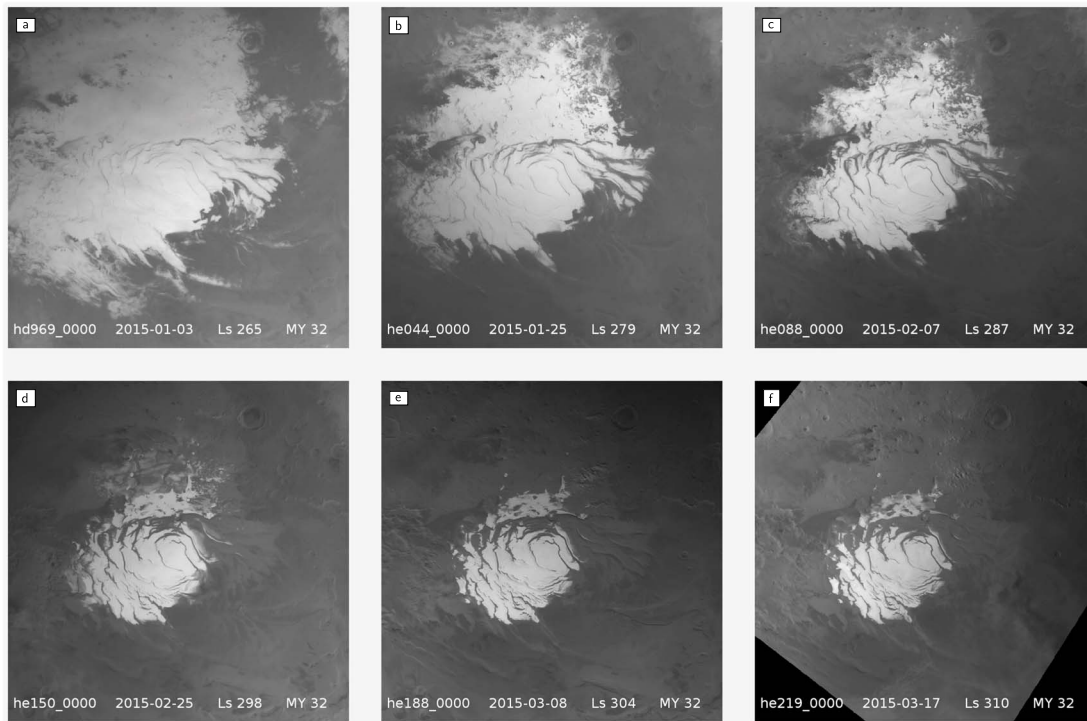
Figure 11. (a–f) Time series of images from the HRSC broom calibration campaign in 2014/2015 (MY 32) showing the retreat of the south polar seasonal cap between Ls 265° and Ls 310°. See supporting information of this paper for an animation of all available images. HRSC = High-Resolution Stereo Camera.

resulting data series of 13 HRSC images show the seasonal retreat of the south polar cap between Ls 260° and Ls 343° of MY 32 in good spatial and temporal detail (Figure 11). After Ls 310° the point of the largest retreat has been hit and the remainder of the images show darkening as the terminator is reaching the polar area in southern winter. An animation of the full set of all 13 images available from the calibration campaign is available in the supporting information of this article.

To compare the interannual seasonal cap recession during different years, Calvin et al. (2017) used an area located at 84°S, 27°E. HRSC image HE188_0000 recorded at Ls 304° in MY 32 (2015) allows the direct comparison with images recorded during the earlier MYs 27 (2005) and 29 (2007) taken near a similar Ls (see Figure 12). The remaining extent of seasonal frost is considerably lower in MY 32 as lower elevation units are brighter in the other two images (see arrow in Figure 12). According to Calvin et al. (2017), the extent of seasonal frost was largest at MY 29 at this spot (cf. Figure 7 of Calvin et al., 2017), but the authors had no Mars Color Imager data available for MY 27. This observation leads to the conclusion that both MY 27 and 29 had slower ice retreat
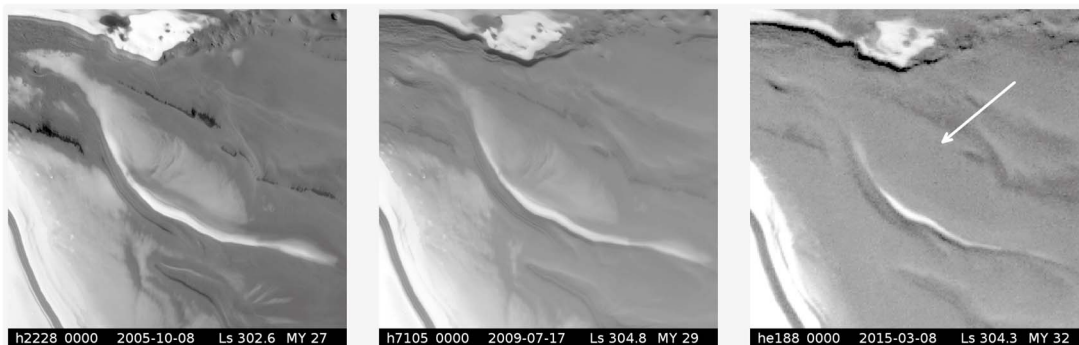

Figure 12. Last retreat of seasonal frost/ice at around Ls 304° for each of three MYs. From left to right MY 27 (2005), MY 29 (2009), and MY 32 (2015). While still present in MYs 27 and 29, the bright deposits have been sublimated in MY 32 (arrow).

rates than usual. In MY 32, the retreat of the seasonal ice/frost deposits at Ls 298° was comparable to that of Ls 304° from the other years (cf. Figure 11d).

4. Summary and Outlook

The iMARS web-GIS is an easy to use but powerful tool to efficiently explore and analyze the single-image and DTM data sets available within the iMars project. With its generally intuitive functions for data exploration it is also well suitable for public outreach purposes. We have implemented novel functionality for time-based single-image visualization which makes it an expert tool for planetary change detection research. It is successfully built upon open-source software components only and supplementary source code is publicly available together with this article. By two independent case studies we have shown that the web-GIS provides unique capabilities for location, visualization, and interpretation of surface change detection features.

Once the results of the automatic change detection routines from within the iMars project are published (Sidiropoulos et al., 2018), they will be included in the web-GIS. The developments shown here will be sustained by other projects such as in a continuation of the HRSC Mapserver (Walter & van Gasselt, 2014). The external access to our dynamic WMS services will be further supported, and additional interfaces to the EPN-TAP interfaces of the Europlanet VO frameworks are planned. Although the project was officially completed in March 2017, the services will be maintained over the next years. It is also planned to extend the application of the tools to other planetary bodies such as Phobos, the Moon and the icy satellites of Saturn.

References

Bailen, M. S., Sucharski, R. M., Akins, S. W., Hare, T. M., & Gaddis, L. R. (2013). Using the PDS Planetary Image Locator Tool (PILOT) to identify and download spacecraft data for research. In *Lunar and Planetary Science Conference* (Vol. 44, pp. 2246).

Broxton, M. J., & Edwards, L. J. (2008). The Ames stereo pipeline: Automated 3D surface reconstruction from orbital imagery. In *Lunar and Planetary Science Conference* (Vol. 39, pp. 2419).

Calvin, W. M., Cantor, B. A., & James, P. B. (2017). Interannual and seasonal changes in the south seasonal polar cap of Mars: Observations from MY 28–31 using MARCI. *Icarus*, *292*, 144–153. https://doi.org/10.1016/j.icarus.2017.01.010

Christensen, P. R., Bandfield, J. L., Hamilton, V. E., Ruff, S. W., Kieffer, H. H., Titus, T. N., et al. (2001). Mars Global Surveyor Thermal Emission Spectrometer experiment: Investigation description and surface science results. *Journal of Geophysical Research*, *106*, 23,823–23,872. https://doi.org/10.1029/2000JE001370

Christensen, P. R., Engle, E., Anwar, S., Dickenshied, S., Noss, D., Gorelick, N., & Weiss-Malik, M. (2009). JMARS—A planetary GIS. In *AGU Fall Meeting Abstracts* (Vol. *22*, pp. IN22A–06).

Clancy, R. T., Sandor, B. J., Wolff, M. J., Christensen, P. R., Smith, M. D., Pearl, J. C., et al. (2000). An intercomparison of ground-based millimeter, MGS TES, and Viking atmospheric temperature measurements: Seasonal and interannual variability of temperatures and dust loading in the global Mars atmosphere. *Journal of Geophysical Research*, *105*(E4), 9553–9571. https://doi.org/10.1029/1999JE001089

Edgett, K. S., & Malin, M. C. (2000). New views of Mars eolian activity, materials, and surface properties: Three vignettes from the Mars Global Surveyor Mars Orbiter Camera. *Journal of Geophysical Research*, *105*(E1), 1623–1650. https://doi.org/10.1029/1999JE001152

Erard, S., Cecconi, B., Le Sidaner, P., Berthier, J., Henry, F., Molinaro, M., et al. (2014). The EPN-TAP protocol for the Planetary Science Virtual Observatory. *Astronomy and Computing*, *7-8*, 52–61. https://doi.org/10.1016/j.ascom.2014.07.008

Gwinner, K., Jaumann, R., Hauber, E., Hoffmann, H., Heipke, C., Oberst, J., et al. (2016). The High Resolution Stereo Camera (HRSC) of Mars Express and its approach to science analysis and mapping for Mars and its satellites. *Planetary and Space Science*, *126*, 93–138. https://doi.org/10.1016/j.pss.2016.02.014

Gwinner, K., Scholten, F., Preusker, F., Elgner, S., Roatsch, T., Spiegel, M., et al. (2010). Topography of Mars from global mapping by HRSC high-resolution digital terrain models and orthoimages: Characteristics and performance. *Earth and Planetary Science Letters*, *294*, 506–519. https://doi.org/10.1016/j.epsl.2009.11.007

Hare, T. M., Archinal, B. A., Plesea, L., Dobinson, E., & Curkendall, D. (2006). Standards proposal to support planetary coordinate reference systems in open geospatial web services and geospatial applications. In *Lunar and Planetary Science Conference* (Vol. 37, pp. 1931).

Hare, T. M., Rossi, A. P., Frigeri, A., & Marmo, C. (2018). Interoperability in planetary research for geospatial data analysis. *Planetary and Space Science*, *150*, 36–42. https://doi.org/10.1016/j.pss.2017.04.004

Heyer, T., Hiesinger, H., Reiss, D., Erkeling, G., Bernhardt, H., Luesebrink, D., & Jaumann, R. (2018). The Multi-Temporal Database of Planetary Image Data (MUTED): A web-based tool for studying dynamic Mars, *159*, 56–65. https://doi.org/10.1016/j.pss.2018.04.015

James, P. B., Thomas, P. C., Wolff, M. J., & Bonev, B. P. (2007). MOC observations of four Mars year variations in the south polar residual cap of Mars. *Icarus*, *192*(2), 318–326. https://doi.org/10.1016/j.icarus.2007.07.014

Keszthelyi, L., Becker, T. L., Sides, S., Barrett, J., Cook, D., Lambright, S., et al. (2013). Support and future vision for the Integrated Software for Imagers and Spectrometers (ISIS). In *Lunar and Planetary Science Conference* (Vol. 44, pp. 2546).

Kieffer, H. H. (2007). Cold jets in the Martian polar caps. *Journal of Geophysical Research*, *112*, E08005. https://doi.org/10.1029/2006JE002816

Kieffer, H. H., Christensen, P. R., & Titus, T. N. (2006). CO_2 jets formed by sublimation beneath translucent slab ice in Mars' seasonal south polar ice cap. *Nature*, *442*(7104), 793–796. https://doi.org/10.1038/nature04945

Kirk, R. L., Howington-Kraus, E., Rosiek, M. R., Anderson, J. A., Archinal, B. A., Becker, K. J., et al. (2008). Ultrahigh resolution topographic mapping of Mars with MRO HiRISE stereo images: Meter-scale slopes of candidate phoenix landing sites. *Journal of Geophysical Research*, *113*, E00A24. https://doi.org/10.1029/2007JE003000

Law, E., & Day, B. (2017). Mars trek: An interactive web portal for current and future missions to Mars. In *European Planetary Science Congress* (Vol. 11, pp. EPSC2017–99).

Loizeau, D., Werner, S. C., Mangold, N., Bibring, J. P., & Vago, J. L. (2012). Chronology of deposition and alteration in the Mawrth Vallis region, Mars. *Planetary and Space Science*, *72*(1), 31–43. https://doi.org/10.1016/j.pss.2012.06.023

Marco Figuera, R., Pham Huu, B., Rossi, A. P., Minin, M., Flahaut, J., & Halder, A. (2018). Online characterization of planetary surfaces: Planetserver, an open-source analysis and visualization tool. *Planetary and Space Science*, *150*, 141–156. https://doi.org/10.1016/j.pss.2017.09.007

Michael, G. G., Walter, S. H. G., Kneissl, T., Zuschneid, W., Gross, C., McGuire, P. C., et al. (2016). Systematic processing of Mars Express HRSC panchromatic and colour image mosaics: Image equalisation using an external brightness reference. *Planetary and Space Science*, *121*, 18–26. https://doi.org/10.1016/j.pss.2015.12.002

Minin, M., Rossi, A. P., Marmo, C., Cecconi, B., Le Sidaner, P., & Erard, S. (2016). Virtual observatory integration of OGC geospatial data and services. In *AGU Fall Meeting Abstracts* (Vol. 31, pp. IN31B–1759).

Moratto, Z. M., Broxton, M. J., Beyer, R. A., Lundy, M., & Husmann, K. (2010). Ames stereo pipeline, Nasa's open source automated stereogrammetry software. In *Lunar and Planetary Science Conference* (Vol. 41, pp. 2364).

Muller, J.-P., Tao, Y., Sidiropoulos, P., Gwinner, K., Willner, K., Fanara, L., et al. (2016). EU-FP7-IMARS: Analysis of Mars multi-resolution images using auto-coregistration, data mining and crowd source techniques: Processed results—A First Look, ISPRS—International Archives of the Photogrammetry. *Remote Sensing and Spatial Information Sciences*, *XLI-B4*, 453–458. https://doi.org/10.5194/isprs-archives-XLI-B4-453-2016

Open Geospatial Consortium (2002). Web map service implementation specification. Version 1.1.1, Open Geospatial Consortium.

Open Geospatial Consortium (2006). OpenGIS® Web Map Server Implementation Specification. OpenGIS Implementation Specification 1.3.0, Open Geospatial Consortium.

Open Geospatial Consortium (2010). OpenGIS Web Feature Service 2.0 Interface Standard. OpenGIS® Implementation Standard, Open Geospatial Consortium.

Piqueux, S., Byrne, S., & Richardson, M. I. (2003). Sublimation of Mars's southern seasonal CO_2 ice cap and the formation of spiders. *Journal of Geophysical Research*, *108*(E8), 5084. https://doi.org/10.1029/2002JE002007

Piqueux, S., & Christensen, P. R. (2008). North and south subice gas flow and venting of the seasonal caps of Mars: A major geomorphological agent. *Journal of Geophysical Research*, *113*, E06005. https://doi.org/10.1029/2007JE003009

Piqueux, S., Kleinböhl, A., Hayne, P. O., Kass, D. M., Schofield, J. T., & McCleese, D. J. (2015). Variability of the Martian seasonal CO_2 cap extent over eight Mars Years. *Icarus*, *251*, 164–180. https://doi.org/10.1016/j.icarus.2014.10.045

Poulet, F., Bibring, J.-P., Mustard, J. F., Gendrin, A., Mangold, N., Langevin, Y., et al. (2005). Phyllosilicates on Mars and implications for early Martian climate. *Nature*, *438*(7068), 623–627. https://doi.org/10.1038/nature04274

Putri, A. R. D., Sidiropoulos, P., & Muller, J.-P. (2016a). Production of HRSC base DTMs for multi-instrument auto coregistration and orthorectification over the Mars south polar region. In *Lunar and Planetary Science Conference* (Vol. 1926, pp. 6071).

Putri, A. R. D., Sidiropoulos, P., & Muller, J.-P. (2016b). Identifying surface changes on HRSC images of the Mars south polar residual cap (SPRC), in: ISPRS—International Archives of the Photogrammetry. https://doi.org/10.5194/isprs-archives-XLI-B4-463-2016

Quinn, P. J, Barnes, D. G., Csabai, I., Cui, C., Genova, F., Hanisch, B., et al. (2004). The international virtual observatory alliance: Recent technical developments and the road ahead. *Proceedings of SPIE*, *5493*, 5493–5493–9. https://doi.org/10.1117/12.551247

Sidiropoulos, P., & Muller, J.-P. (2017). Automatic detection of changes on Mars surface from high-resolution orbital images. In *EGU General Assembly Conference Abstracts* (Vol. 19, pp. 18300). EGU General Assembly Conference Abstracts.

Sidiropoulos, P., & Muller, J.-P. (2018). A systematic solution to multi-instrument coregistration of high-resolution planetary images to an orthorectified baseline. *IEEE Transactions on Geoscience and Remote Sensing*, *56*(1), 78–92. https://doi.org/10.1109/TGRS.2017.2734693

Sidiropoulos, P., Muller, J.-P., Watson, G., Michael, G., & Walter, S. (2018). Automatic coregistration and orthorectification (ACRO) and subsequent mosaicing of NASA high-resolution imagery over the Mars MC11 quadrangle, using HRSC as a baseline. *Planetary and Space Science*, *151*, 33–42. https://doi.org/10.1016/j.pss.2017.10.012

Smith, D. E., Zuber, M. T., Frey, H. V., Garvin, J. B., Head, J. W., Muhleman, D. O., et al. (2001). Mars orbiter laser altimeter: Experiment summary after the first year of global mapping of Mars. *Journal of Geophysical Research*, *106*(E10), 23,689–23,722. https://doi.org/10.1029/2000JE001364

Smith, D., Zuber, M., Neumann, G., Guinness, E. A., & Slavney, S. (2003). Mars global surveyor laser altimeter mission experiment gridded data record. MGS-M-MOLA,-5-MEGDR-L3-V1.0.

Sprinks, J. C., Wardlaw, J., Houghton, R., Bamford, S., & Marsh, S. (2016a). Mars in motion: An online citizen science platform looking for changes on the surface of Mars. In *AAS/Division for Planetary Sciences Meeting Abstracts* (Vol. 48, pp. 426.01).

Sprinks, J. C., Wardlaw, J., Houghton, R., Bamford, S., & Marsh, S. (2016b). Better the Martian you know? Trust in the crowd vs. trust in the machine when using a Martian citizen science platform. In *AAS/Division for Planetary Sciences Meeting Abstracts* (Vol. 48, pp. 406.02).

Tao, Y., & Muller, J.-P. (2016). An optimised system for generating multi-resolution DTMs using NASA MRO datasets. *ISPRS - International Archives of the Photogrammetry, Remote Sensing and Spatial Information Sciences*, *XLI-B3*, 115–121. https://doi.org/10.5194/isprsarchives-XLI-B3-115-2016

Tao, Y., Muller, J.-P., & Poole, W. (2016). Automated localisation of Mars rovers using co-registered HiRISE-CTX-HRSC orthorectified images and wide baseline Navcam orthorectified mosaics. *Icarus*, *280*, 139–157. https://doi.org/10.1016/j.icarus.2016.06.017

Tao, Y., Muller, J.-P., Sidiropoulos, P., Putri, K., Campbell, J., & Walter, S. (2018). Assessment of ≈5,000 Mars-wide CTX DTMs created using the EU-FP7 iMars CASP-GO system. In *EGU General Assembly Conference Abstracts, EGU General Assembly Conference Abstracts*, *19*, 15971.

Tao, Y., Muller, J. P., Sidiropoulos, P., Xiong, S.-T., Putri, A. R. D., Walter, S. H. G., et al. (2018). Massive stereo-based DTM production for Mars on cloud computers. *Planetary and Space Science*. https://doi.org/10.1016/j.pss.2018.02.012

Thomas, P., & Veverka, J. (1979). Seasonal and secular variation of wind streaks on Mars: An analysis of Mariner 9 and Viking data. *Journal of Geophysical Research*, *84*(B14), 8131–8146. https://doi.org/10.1029/JB084iB14p08131

Walter, S. H. G., Gasselt, S. V., Michael, G., & Neukum, G. (2006). Footprint representation of planetary remote sensing data. In *European Planetary Science Congress 2006* (pp. 508).

Walter, S. H. G., Michael, G., Gasselt, S. v., & Kneissl, T. (2015). Photometric Lambert correction for global mosaicking of HRSC image data. In *Lunar and Planetary Science Conference* (Vol. 46, pp. 1434).

Walter, S. H. G., & van Gasselt, S. (2014). HRSC data dissemination—Dynamic queries and data interoperability. In *Lunar and Planetary Science Conference* (Vol. 45, pp. 1088).

Wang, J., Bennett, K. J., Scholes, D., Arvidson, R., Ward, J. G., Slavney, S., et al. (2009). Planetary data access through the orbital data explorer from the PDS geosciences node. In *Lunar and Planetary Science Conference* (Vol. 40, pp. 1193).